BV-G COLOR-IMAGE DECOMPOSITION WITH ITS APPLICATION TO IMAGE PROCESSING OF A DIGITAL COLOR CAMERA

Takahiro Saito, Daisuke Yamada, and Takashi Komatsu

Department of E&I Frontiers, High-Tech Research Center, Kanagawa University
3-27-1 Rokkakubashi, Kanagawa-ku, 221-8686, Yokohama, Japan
phone: + (81) 45 481 5661, fax: + (81) 45 491 7915, email: saitot01@kanagawa-u.ac.jp
web: http://slat4.ee.kanagawa-u.ac.jp

ABSTRACT

This paper extends the BV (Bounded Variation) - G variational nonlinear image-decomposition approach, which is considered to be useful for image processing of a digital color camera, to a genuine color-image decomposition approach. For utilizing inter-channel color cross-correlations, this paper introduces TV (Total Variation) norms of color differences and TV norms of color sums into the BV-G energy functionals, and then derives a denoising-type decomposition-algorithm with over-complete wavelet transform, through applying the Besov-norm approximation to the variational problem. Our method decomposes a noisy color image without producing undesirable low-frequency colored artifacts in its separated BV-component, and achieves desirable high-quality color-image decomposition, which is robust against colored random noise. Furthermore, this paper applies this color-image decomposition method to an IP (Image-Processing) - pipeline of a digital color camera, and the application enables the IP-pipeline to adjust a quality trade-off between texture sharpness and noise visibility according to user's taste.

1. INTRODUCTION

Previously we have presented the decomposition-based image-processing approach and showed its advantages over the conventional image-processing approach [1], [2]. The approach firstly decomposes an input image into its components, and then processes each separated component independently with an image-processing method suitable to it. As the image-decomposition method for image processing of a digital color camera, we have studied the BV (Bounded Variation) - G variational image-decomposition approach [3].

The BV-G variational image-decomposition approach decomposes an input image into its BV component corresponding to a structural image-approximation and its G component corresponding to image textures, and is suitable for image processing of an image taken with a digital camera [2]. However, this variational image-decomposition approach was proposed originally for a monochrome image, and decomposes each primary color channel separately [3]. Since inter-channel color cross-correlations are not taken into account for decomposing a color image, image textures are not completely removed from its separated BV component, and the BV component is sometimes smeared with low-frequency colored artifacts.

To improve the image-decomposition and to remove the low-frequency colored artifacts from the separated BV components, this paper extends the existing BV-G variational image-decomposition approach to a genuine color-image decomposition approach. For utilizing inter-channel color cross-correlations for the image-decomposition, this paper introduces TV (Total Variation) norms of color differences and TV norms of color sums into the energy functional to be minimized, replaces the TV norms by the Besov norms, defined in an over-complete wavelet transform domain, and then derives a new denoising-type alternately iterative decomposition algorithm with over-complete wavelet transform. Our new color-image decomposition method succeeds in decomposing an input color-image without producing the low-frequency colored artifacts in the separated BV component, removes oscillatory textures from the separated BV component almost completely, and achieves high-quality decomposition, which is robust against colored random noise.

Furthermore, this paper applies our new color-image decomposition method to an IP (image processing) - pipeline of a digital color camera, and experimentally shows the superiority over the existing standard IP-pipeline. Our new IP-pipeline can adjust a trade-off in picture quality between texture sharpness and noise visibility according to user's taste.

2. BV-G VARIATIONAL IMAGE-DECOMPOSITION MODEL AND ITS SOLUTION

The BV-G variational image-decomposition model to decompose an input image into its structural component and its texture component was proposed originally for a monochrome image [3].

2.1 BV-G Variational Image-Decomposition Model

The BV-G variational image-decomposition model decomposes an input image f into a sum of its BV component u and its G component v. The BV component u, also referred to as the structure component, is modeled as an intensity variation corresponding to geometrical structures characterizing the image f, whereas the G component v, also referred to as the texture component, is modeled as an oscillatory intensity variation corresponding to textures of the image f. By defining the norms of the BV component u and the G component v by the TV norm $J(u)$ and the G norm $\|v\|_G$ respectively, the image-decomposition problem is formulated as the following variational problem [3]:

$$\inf_{u,v}\left(J(u)+\frac{1}{2\eta}\left\|f-u-v\right\|_2^2\right),\ \eta>0,\ \mu>0,\quad \text{subject to } v\in G_\mu=\left\{v\ \middle|\ \|v\|_G\le\mu\right\}, \tag{1}$$

where the TV norm $J(u)$, the G norm $\|v\|_G$ and the L^2 norm $\|f-u-v\|_2^2$ are defined by

$$J(u)=\int_\Omega|\nabla u|\,d\Omega \quad :\text{TV norm}, \tag{2}$$

$$\|v\|_G=\inf\left\{\ \|\mathbf{g}\|_\infty\ \middle|\ v=div(\mathbf{g})\ \right\} \quad :\text{G norm}, \tag{3}$$

$$\|\mathbf{g}\|_\infty=\sup_{x\in\Omega}|\mathbf{g}(x)|,\quad \mathbf{g}=(g_1,g_2)^T,$$

$$\left\|f-u-v\right\|_2^2=\int_\Omega|f-u-v|^2\,d\Omega \quad :L^2\ \text{norm}. \tag{4}$$

The parameter η in (1) corresponds to energy of residuals $f - u - v$, and, for a noisy input f, the value of η is set so that its value may be proportional to the noise variance. The variational problem of (1) can be converted into its equivalent variational problem:

$$\inf_{u,v}\left(J(u) + J^*\left(\frac{v}{\mu}\right) + \frac{1}{2\eta}\left\| f-u-v \right\|_2^2 \right),\ \eta>0,\ \mu>0, \quad (5)$$

$$J^*(v) = \mathcal{X}_{G_1}(v) = \begin{cases} 0 & if\ \ v \in G_1, \\ +\infty & if\ \ v \notin G_1. \end{cases}$$

The functional J^* is the indicator functional of the closed convex set G_1. Since the functional of (5) is coercive and it is strictly convex except in the direction $(u, v) = (u, -v)$, the variational problem of (5) admits a unique solution $(\hat{u},\hat{v})$ [3]. Solving the variational problem of (5) is equivalent to solving the following two variational strictly convex sub-problems simultaneously.

[Variational sub-problem 1]

The G component v being fixed, the BV component u is sought as a solution of the variational sub-problem:

$$\inf_u\left(J(u) + \frac{1}{2\eta}\left\| f-u-v \right\|_2^2 \right). \quad (6)$$

[Variational sub-problem 2]

The BV component u being fixed, the G component v is sought as a solution of the variational sub-problem:

$$\inf_v\left(\left\| f-u-v \right\|_2^2 \right),\ \text{subject to } v \in G_\mu. \quad (7)$$

2.2 Projection-type Alternately Iterative Algorithm

In [3], it was proved that the sub-problems of (6) and (7) have a unique solution identical to the unique solution of (5), and that the unique solution is provided with the Chambolle projection algorithm. The solution of the variational sub-problem of (6) is given by

$$\tilde{u} = f - v - P_\eta(f - v), \quad (8)$$

where the operator P_η is the convex projector onto the closed convex set G_η. The convex projection P_η is computed by solving the following minimization problem with the classical semi-implicit gradient descent algorithm:

$$\min_{\mathbf{p}}\left\{ \left\| \rho \cdot div(\mathbf{p}) - f \right\|_2^2 \right\},\ \text{subject to } |\mathbf{p}| \le 1 \text{ on } \Omega. \quad (9)$$

On the other hand, the solution of the variational sub-problem of (7) is given by

$$\tilde{v} = P_\mu(f - u), \quad (10)$$

where the operator P_μ is the convex projector onto the closed convex set G_μ.

The variational problem of (5) is solved by the following algorithm [3].

[Projection-type Alternately Iterative Algorithm]

1) Initialization: $\tilde{u}^{(0)} = \tilde{v}^{(0)} = 0,\ \ n = 0,\ \ \varepsilon > 0$

2) Iteration:

2-1) Projection 1: $\tilde{u}^{(n+1)} = f - \tilde{v}^{(n)} - P_\eta\left(f - \tilde{v}^{(n)}\right)$

2-2) Projection 2: $\tilde{v}^{(n+1)} = P_\mu\left(f - \tilde{u}^{(n+1)}\right)$

2-3) Convergence test: we will stop the iteration if

$$\max\left\{ \left|\tilde{u}^{(n+1)} - \tilde{u}^{(n)}\right|, \left|\tilde{v}^{(n+1)} - \tilde{v}^{(n)}\right| \right\} \le \varepsilon$$

; otherwise, $n \leftarrow n+1$, and we will return to 2-1). [End]

The convergence of the algorithm is guaranteed, and the sequence $(\tilde{u}^{(n)}, \tilde{v}^{(n)})$ necessarily converges to the unique solution of (5) [3].

2.3 Denoising-type Alternately Iterative Algorithm in an Over-complete Wavelet Transform Domain

It is difficult to solve the variational sub-problem of (7) directly without the Chambolle projection algorithm. However, unlike the variational sub-problem of (7), its dual variational sub-problem is easily solved directly without the Chambolle projection algorithm. If we define an auxiliary function $\tilde{w}$ as $\tilde{w} = f - u - \tilde{v}$ where $\tilde{v}$ is the solution of (7), then the function $\tilde{w}$ will necessarily be a solution of the following variational sub-problem [5]:

$$\inf_w\left(J(w) + \frac{1}{2\mu}\left\| f-u-w \right\|_2^2 \right). \quad (11)$$

Instead of solving the variational sub-problem of (7) directly, we search for the solution $\tilde{w}$ of its dual variational sub-problem of (11), and then we compute the solution $\tilde{v}$ of (7) as $\tilde{v} = f - u - \tilde{w}$. Both the two variational sub-problems of (6) and (11) to be solved simultaneously are typical TV-denoising problems, but their direct TV minimization needs a vast amount of computations. Instead of solving their Euler-Lagrange equations directly, we firstly introduce the Besov-norm approximation [6] that the TV norm $J(f)$ is coarsely approximated by the Besov norm $\| f \|_{B^1_{1,1}}$ defined as

$$\left\| f \right\|_{B^1_{1,1}} = \sum_{j\in Z}\sum_{(k,l)\in Z^2}\left| F_{j,k,l} \right|, \quad (12)$$

$F_{j,k,l}$: Wavelet transform coefficient of f,

and then we approximately solve the two variational sub-problems of (6) and (11) with the two different wavelet shrinkage denoising methods in the over-complete wavelet transform domain that is constructed from orthonormal wavelet transform such as the Haar wavelet transform. The two simultaneous variational sub-problems of (6) and (11) have a unique solution identical to the unique solution $(\hat{u},\hat{v})$ of (5) [5], but the denoising-type solution with the over-complete wavelet transform merely provides a coarse approximation to the unique solution.

The variational problem of (5) is approximately solved by the following algorithm with the over-complete wavelet transform.

[Denoising-type Alternately Iterative Algorithm with the Over-complete Wavelet Transform]

1) Initialization: $\tilde{u}^{(0)} = \tilde{v}^{(0)} = 0,\ \ n = 0,\ \ \varepsilon > 0$

2) Iteration:

2-1) Denoising 1: we denoise $f - \tilde{v}^{(n)}$ by the wavelet shrinkage denoising method using the soft-thresholding function ST of (13) with the threshold parameter η, which is identical to η in (6) and is common to all the wavelet coefficients, and we regard its denoised output as the solution $\tilde{u}^{(n+1)}$ of (6).

$$y = \mathrm{ST}(x;\eta) = \begin{cases} x-\eta, & f\ \ x > \eta, \\ 0\ , & if\ \ -\eta \le x \le \eta, \\ x+\eta, & if\ \ x < -\eta. \end{cases} \quad (13)$$

2-2) Denoising 2: we denoise $f - \tilde{u}^{(n+1)}$ by the wavelet shrinkage denoising method using the soft-thresholding function ST with the threshold parameter μ, which is identical to μ in (11) and is common to all the wavelet coefficients, and then from its denoised output $\tilde{w}$ we compute $\tilde{v}^{(n+1)}$ as $\tilde{v}^{(n+1)} = f - \tilde{u}^{(n+1)} - \tilde{w}$.

2-3) Convergence test: we will stop the iteration if the above-mentioned convergence condition is satisfied; otherwise, $n \leftarrow n+1$, and we will return to 2-1). [End]

The algorithm always converges to a coarse approximation of the unique solution of (5).

3. BV-G VARIATIONAL COLOR-IMAGE DECOMPOSITION MODEL AND ITS SOLUTION

To improve the image-decomposition, this paper extends the existing BV-G variational image-decomposition approach to a genuine

color-image decomposition approach that utilizes inter-channel color cross-correlations.

3.1 BV-G Variational Color-Image Decomposition Model

If we apply the BV-G variational image-decomposition approach described in Sec. 2 separately to each primary color channel of a noisy color image, oscillatory intensity variation will not be completely removed from its separated BV component, and low-frequency colored artifacts will often appear in its separated BV component, and it will not necessarily produce desirable decomposition results. Random noise has little inter-channel color cross-correlation among the three primary color channels, whereas a noise-free natural color image has a strong inter-channel color cross-correlation. To remove the low-frequency colored artifacts from the separated BV component, we should utilize those properties of the inter-channel color cross-correlation for decomposing a color image. Previously, we proposed TV norms of color differences and TV norms of color sums as a mathematical tool to utilize inter-channel color cross-correlations for the variational formulation [7]. In this paper, we introduce the TV norms of color differences and the TV norms of color sums into the norm definition of the BV component, and thus we formulate the BV-G color-image decomposition problem as the following variational problem:

$$\inf_{\substack{u_r,u_g,u_b\\ v_r,v_g,v_b}} \left\{ J(u_r)+J(u_g)+J(u_b)+\alpha\cdot J(u_r-u_g)+\beta\cdot J(u_r+u_g) \right.$$
$$+\alpha\cdot J(u_g-u_b)+\beta\cdot J(u_g+u_b)+\alpha\cdot J(u_b-u_r)+\beta\cdot J(u_b+u_r) \quad (14)$$
$$\left. +\frac{\lambda}{2}\|f_r-u_r-v_r\|_2^2+\frac{\lambda}{2}\|f_g-u_g-v_g\|_2^2+\frac{\lambda}{2}\|f_b-u_b-v_b\|_2^2 \right\}$$
$$\text{subject to } v_r,v_g,v_b\in G_\mu ; \qquad \mu>0,\ \lambda>0,\ \alpha>\beta\geq 0,$$

f_r,f_g,f_b : RGB three primary color signals,

u_r,u_g,u_b : BV components for RGB,

v_r,v_g,v_b : G components for RGB.

Since the functional of (14), as well as the functionals of (1) and (5) [3], is coercive and is strictly convex except in the direction, $(u_c, v_c) = (u_c, -v_c)$, $(c = r, g, b)$, the problem of (14) has a unique solution.

3.2 Denoising-type Alternately Iterative Algorithm in an Over-complete Wavelet Transform Domain

Unlike the original BV-G variational image-decomposition problem of (1), the BV-G variational color-image decomposition problem of (14) cannot be solved with the Chambolle projection algorithm. As described in Sec. 2.3, we solve the variational problem of (14) approximately with a denoising-type alternately iterative algorithm in the over-complete wavelet transform domain.

We convert the problem of (14) into its two variational sub-problems of (15) and (16). Since the functionals of (15) and (16) are coercive and strictly convex, the sub-problems of (15) and (16) have a unique solution identical to the unique solution of (14).

[Variational sub-problem 1]

The three G components, v_r, v_g and v_b, being fixed, the three BV components, u_r, u_g and u_b, are sought as a solution of the variational sub-problem:

$$\inf_{u_r,u_g,u_b} \left\{ J(u_r)+J(u_g)+J(u_b)+\alpha\cdot J(u_r-u_g)+\beta\cdot J(u_r+u_g) \right.$$
$$+\alpha\cdot J(u_g-u_b)+\beta\cdot J(u_g+u_b)+\alpha\cdot J(u_b-u_r)+\beta\cdot J(u_b+u_r) \quad (15)$$
$$\left. +\frac{\lambda}{2}\|f_r-u_r-v_r\|_2^2+\frac{\lambda}{2}\|f_g-u_g-v_g\|_2^2+\frac{\lambda}{2}\|f_b-u_b-v_b\|_2^2 \right\}.$$

The variational sub-problem 1 is a kind of color-image denoising problem where the three primary color channels are collectively denoised. Previously, we derived its approximate solution in the over-complete wavelet transform domain as a color-image denoising method [8]. We attain to the approximate solution of (15) by applying our previously proposed wavelet color shrinkage denoising method using the l^1-l^2 color shrinkage scheme [8], collectively to the three primary color signals, $f_r - v_r$, $f_g - v_g$ and $f_b - v_b$.

[Variational sub-problem 2]

The three BV components, u_r, u_g and u_b, being fixed, the three G components, v_r, v_g and v_b, are sought as solutions of the variational sub-problems:

$$\inf_{v_c}\left(\|f_c-u_c-v_c\|_2^2 \right), \text{ subject to } v_c\in G_\mu ;\ c=r,g,b. \quad (16)$$

The sub-problem 2 consists of the three independent problems for the three primary color channels, and the three problems are of the identical type to the variational problem of (7). Their dual problems amount to the following variational denoising problems:

$$\inf_{w_c}\left(J(w_c)+\frac{1}{2\mu}\|f_c-u_c-w_c\|_2^2 \right);\ c=r,g,b, \quad (17)$$
$$w_c = f_c-u_c-v_c.$$

The variational denoising problems are solved approximately with the wavelet shrinkage denoising method using the soft-thresholding function ST of the threshold parameter $\mu > 0$.

The variational problem of (14) is approximately solved by the following algorithm with the over-complete wavelet transform.

[Denoising-type Alternately Iterative Algorithm with the Over-complete Wavelet Transform]

1) Initialization: $\tilde{u}_c^{(0)}=\tilde{v}_c^{(0)}=0 \quad (c=r,g,b)$, $\quad n=0$, $\quad \varepsilon>0$

2) Iteration:

2-1) Denoising 1: we denoise the three primary color signals, $f_c-\tilde{v}_c^{(n)}, (c=r,g,b)$, collectively by the wavelet color shrinkage denoising method using the l^1-l^2 color shrinkage scheme, and its denoised outputs, $\tilde{u}_c^{(n+1)}, (c=r,g,b)$, correspond to coarse approximations of the solutions of (15).

2-2) Denoising 2: we denoise each of $f_c-\tilde{u}_c^{(n+1)}, (c=r,g,b)$, separately by the wavelet shrinkage denoising method using the soft-thresholding function ST with the threshold parameter μ, and then from their denoised outputs, $\tilde{w}_r$, $\tilde{w}_g$, and $\tilde{w}_b$, we compute the three primary signals, $\tilde{v}_c^{(n+1)}, (c=r,g,b)$, as $\tilde{v}_c^{(n+1)}=f_c-\tilde{u}_c^{(n+1)}-\tilde{w}_c$, which correspond to coarse approximations of the solutions of (16).

2-3) Convergence test: we will stop the iteration if

$$\max\left\{ \left|\tilde{u}_c^{(n+1)}-\tilde{u}_c^{(n)}\right|, \left|\tilde{v}_c^{(n+1)}-\tilde{v}_c^{(n)}\right| \right\}\leq\varepsilon \quad ;\ c=r,g,b$$

; otherwise, $n\leftarrow n+1$, and we will return to 2-1). [End]

Since update at each iteration step is non-expansive mapping defined on the closed convex set, the above algorithm always converges; and the convergent result corresponds to a coarse approximation of the unique solution of (14).

3.3 Evaluations of Decomposition Performance

We apply our BV-G color-image decomposition method to both noise-free test color images and noisy test color images, which we produce by adding signal-dependent noise equivalent to the ISO 1600 sensitivity [8]. Our method employs the un-decimated Haar wavelet transform as over-complete wavelet transform.

(a) Noise-free test color image (b) Noisy test color image

Figure 1 – Test color images.

Fig. 2 and Fig. 3 compare the BV component and the G component provided by our color-image decomposition method with those provided by the existing BV-G image-decomposition method [3] with the Chambolle projection algorithm [4]. Since the existing method does not utilize inter-channel color cross-correlations, it does not completely remove oscillatory intensity variations from its separated BV component even for the noise-free image, and particularly for the noisy image it produces noticeable colored artifacts in its separated BV component. On the other hand, our method successfully takes away the oscillatory intensity variations and the colored artifacts from its separated BV component almost perfectly, and the BV component separated from the noisy image is almost the same as that separated from the noise-free image; whereas most of additive colored noise in the noisy input color image is separated as its G component.

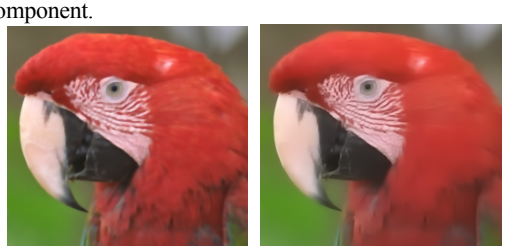

(a) BV component separated by the existing method [3] (b) BV component separated by our method

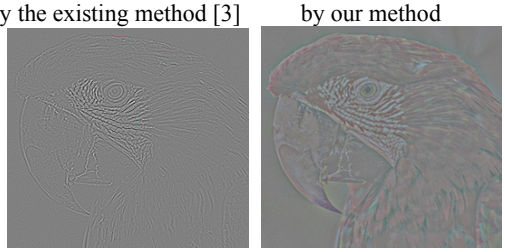

(c) G component separated by the existing method [3] (d) G component separated by our method

Figure 2 – Decomposition results for the noise-free test color image.

(a) BV component separated by the existing method [3] (b) BV component separated by our method

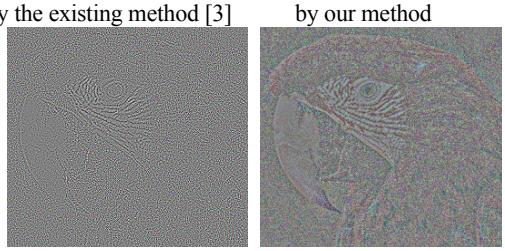

(c) G component separated by the existing method [3] (d) G component separated by our method

Figure 3 – Decomposition results for the noisy test color image.

4. APPLICATION TO IMAGE PROCESSING OF A DIGITAL COLOR CAMERA

4.1 Decomposition-Based Image-Processing Pipeline

The standard IP-pipeline, in which demosaicing is followed by white balancing, color enhancement, and inverse gamma correction [9], does not necessarily recover a high-quality color image. In a practical noisy-observation case, the standard IP-pipeline tends to weaken the visibility of textures in bright image regions, and at the same time it tends to increase the visibility of colored noise in dark image regions, which is believed to be common drawbacks to a digital color camera. Those drawbacks are caused by the standard IP-pipeline rather than by the color-imaging scheme itself. To remedy the drawbacks, firstly texture components should be separated, and then the texture components should be retouched adaptively while taking into account signal dependency of the noise. This paper puts this idea into shape, and thus proposes a decomposition-based IP-pipeline whose flow diagram is shown in Fig. 4.

The decomposition-based IP-pipeline firstly interpolates observed raw color data with a proper demosaicing method. The color-data are contaminated by observation noise, and are blurred by an optical low-pass filter and a sample-hold process. To achieve efficient demosaicing, we need to take the effects of the noise and the blur into account, and hence we employ our extended color-TV-regularization deblurring-demosaicing method [7].

The decomposition-based approach decomposes the demosaicked image f with the BV-G color-image decomposition method. Most of the observation noise mingles with the separated G component v, whereas the BV component u is little affected by the noise.

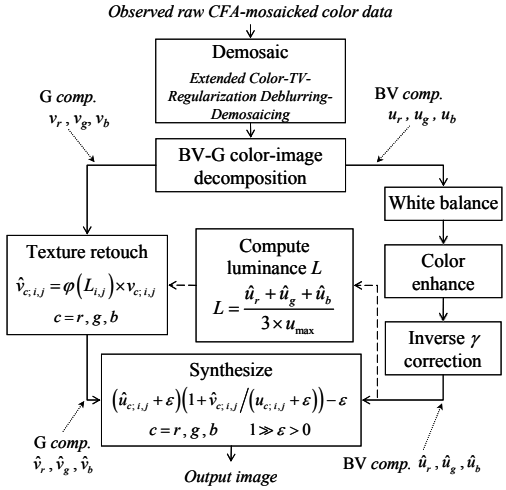

Figure 4 – Decomposition-based IP-pipeline.

Unlike the standard IP-pipeline, white balancing, color enhancement and inverse gamma correction are applied only to the separated BV components, u_r, u_g, u_b, of the three primary color channels. On the other hand, the separated G components, v_r, v_g, v_b, of the three primary color channels are retouched by utilizing the processed BV components, $\hat{u}_r$, $\hat{u}_g$, $\hat{u}_b$, to adjust a trade-off between noise visibility and texture sharpness, as follows:

1) for each pixel at (i, j), a normalized luminance value $L_{i,j}$ is computed by

$$L_{i,j} = \frac{\left(\hat{u}_r + \hat{u}_g + \hat{u}_b\right)_{i,j}}{3 \times u_{\max}}, \quad 0 \le L_{i,j} \le 1, \tag{18}$$

where u_{max} is the maximum value of u.

2) a weighting coefficient φ is determined by

$$\varphi\left(L_{i,j}\right) = 1.0 - c_1 \cdot L_{i,j} \exp\left(-4L_{i,j}\right), \quad 0 \le c_1 \le 4e, \tag{19}$$

where c_1 is used to control the texture retouch. The proper value of c_1 depends on the intensity of observation noise. As the noise increases in intensity, the parameter c_1 should be given a higher value.

3) v_r, v_g, and v_b, are retouched by

$$\hat{v}_{c;i,j} = \varphi\left(L_{i,j}\right) \times v_{c;i,j}, \qquad c = r, g, b. \tag{20}$$

$\varphi(L)$ is nonnegative within the range $0 \le L \le 1$ and has the minimum value $1 - c_1/(4e)$ at $L = 1/4$. The texture retouch of (20) weakens magnitude of variations in v_r, v_g, and v_b in dark image regions where L is in the vicinity of 1/4. This property of φ is based on a well-known fact that noise is the most noticeable in dark image regions where the normalized signal intensity is around 1/4 [8]. The texture retouch somewhat suppresses original image textures, but alleviates the bad effects of noise, dominant in dark image regions. On the other hand, in bright image regions where L is close to 1, since $\varphi(L)$ has a value close to 1, v_r, v_g, and v_b are scarcely retouched.

After these IP tasks, combining the processed BV components and the processed G components into an output color image:

$$\hat{f}_{i,j} = \left(\hat{u}_{c;\,i,j} + \varepsilon\right)\left(1 + \hat{v}_{c;\,i,j} \Big/ \left(u_{c;\,i,j} + \varepsilon\right)\right) - \varepsilon\,, \quad c = r\,, g\,, b\,, \quad (21)$$

where ε is a small positive value to prevent singularity at $u_c = 0$.

4.2 Evaluations of the IP-pipeline

Fig. 5 shows the same portions of color images given by our new decomposition-based IP-pipeline and the standard IP-pipeline with our extended color-TV-regularization deblurring-demosaicing method [7], to raw mosaicked-color-data, which are read out from a digital SLR camera and are scarcely contaminated with observation noise. In Fig. 5, the parameter c_1 is fixed at 0.0, namely, no texture retouch is performed. The standard IP-pipeline does not restore fine image textures in bright image regions, and produces a color image giving a somewhat blurry impression; whereas our new IP-pipeline restores those fine image textures, and produces a color image giving a shaper visual impression.

To evaluate robustness against observation noise, we produce noisy color-data by adding artificially generated shot-noise to the observed raw color-data, and apply our new IP-pipeline to the noisy color-data. Fig. 6 compares the same portions of color images. The standard IP-pipeline suppresses the visibility of textures in bright image regions, and forms false colored artifacts in dark image regions. Our new IP-pipeline produces a sharper color image, and simultaneously suppresses the false colored artifacts in dark image regions when the parameter c_1 is properly set. From the point of a balance of texture sharpness and noise visibility, our new IP-pipeline performs better for real noisy mosaicked-color-data.

5. CONCLUSIONS

This paper extends the BV-G variational nonlinear image-decomposition approach, originally proposed for a monochrome image, to a genuine color-image decomposition approach. Furthermore, this paper applies this color-image decomposition method to an IP-pipeline of a digital color camera, and our new decomposition-based IP-pipeline achieves a better trade-off in picture quality between texture sharpness and noise visibility.

REFERENCES

[1] T. Saito, Y. Ishii, Y. Nakagawa and T Komatsu, "Adaptable image interpolation with skeleton-texture separation," in *Proc. 2006 IEEE Int. Conf. Image Processing*, pp.681-684, 2006.

[2] T. Saito, Y. Ishii, H. Aizawa, D. Yamada, and T. Komatsu, "Nonlinear decomposition-and-demosaicing approach for a digital color camera," in *Proc. EUSIPCO 2008*, 1569098794.pdf, 2008.

[3] J.-F.Aujol, G. Aubert, L. Blanc-Feraud, and A. Chambolle, "Image decomposition into a bounded variation component and an oscillating component," J*ournal of Mathematical Imaging and Vision*, vol.22, no.1, pp.71-88, 2005.

[4] A. Chambolle, "An algorithm for total variation minimization and applications," *Journal of Mathematical Imaging and Vision*, vol.20, no.1/2, pp.89-97, 2004.

[5] J.-F. Aujol and S.H. Kang, "Color image decomposition and restoration," *J. Visual Communication and Image Representation*, vol.17, no.4, pp.916-928, 2006.

[6] A. Chambolle, R.A. De Vore, N. Lee, and B.J. Lucier, "Nonlinear wavelet image processing: variational problems, compression, and noise removal through wavelet shrinkage," *IEEE Trans. Image Processing*, vol.7, no.3, pp.319-335, 1998.

[7] T. Saito, T. Komatsu, "Demosaicing approach based on extended color total-variation regularization," in *Proc. of 2008 IEEE Int. Conf. on Image Processing*, pp.885-888, 2008.

[8] T. Saito and T. Komatsu, "Total-variation approach and wavelet shrinkage for color-image denoising with inter-channel color cross-correlations," in *Proc. IEEE 3rd Int. Symposium on Communication, Control and Signal Processing*, pp.494-499, 2008.

[9] R. Ramanath, W. E. Synder, Y. Yoo, and M. S. Drew, "Color image processing pipeline," *IEEE Signal Processing Magazine*, vol.22, no.1, pp.34-43, 2005.

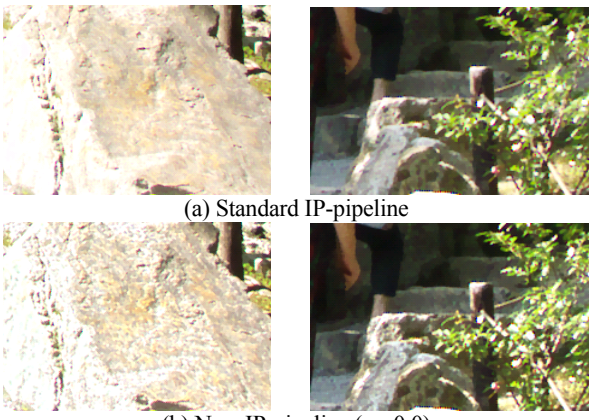

(a) Standard IP-pipeline

(b) New IP-pipeline (c_1=0.0)

Figure 5 – Portions of color images restored from raw mosaicked-color-data, scarcely contaminated with observation noise, by the standard IP-pipeline and our new IP-pipeline.

(a) Standard IP (b) New IP (c_1 = 0.0) (c) New IP (c_1 = 2.0)

(d) New IP (c_1 = 4.0) (e) New IP (c_1 = 6.0) (f) New IP (c_1 = 8.0)

Figure 6 – Portions of color images restored from noisy mosaicked-color-data by the standard IP-pipeline and our new IP-pipeline in which the parameter c_1 is varied.